Nucleolar Molecular Signature of Pluripotent Stem Cells

ARTICLE *in* ANALYTICAL CHEMISTRY · MARCH 2013

Impact Factor: 5.64 · DOI: 10.1021/ac303806j · Source: PubMed

8 AUTHORS, INCLUDING:

Artem Pliss
University at Buffalo, The State University of N…
44 PUBLICATIONS **487** CITATIONS
SEE PROFILE

Andrey N. Kuzmin
University at Buffalo, The State University of N…
90 PUBLICATIONS **1,260** CITATIONS
SEE PROFILE

Aliaksandr V. Kachynski
University at Buffalo, The State University of N…
71 PUBLICATIONS **917** CITATIONS
SEE PROFILE

Zhixing hu
15 PUBLICATIONS **139** CITATIONS
SEE PROFILE

analytical chemistry

Article

pubs.acs.org/ac

Nucleolar Molecular Signature of Pluripotent Stem Cells

Artem Pliss,[†] Andrey N. Kuzmin,[†] Aliaksandr V. Kachynski,[†] Houbo Jiang,[‡] Zhixing Hu,[‡] Yong Ren,[‡] Jian Feng,[‡] and Paras N. Prasad*[,†,§,∥]

[†]Institute for Lasers, Photonics and Biophotonics, University at Buffalo, State University of New York, Buffalo, New York 14260, United States

[‡]Department of Physiology and Biophysics, University at Buffalo, State University of New York, Buffalo, New York 14214, United States

[§]Department of Chemistry, University at Buffalo, State University of New York, Buffalo, New York 14260, United States

[∥]Department of Chemistry, Korea University, Seoul, 136-701, Korea

Supporting Information

ABSTRACT: Induced pluripotent stem cells (iPSC) are generated by reprogramming somatic cells to the pluripotent state. Identification and quantitative characterization of changes in the molecular organization of the cell during the process of cellular reprogramming is valuable for stem cell research and advancement of its therapeutic applications. Here we employ quantitative Raman microspectroscopy and biomolecular component analysis (BCA) for a comparative analysis of the molecular composition of nucleoli in skin fibroblasts and iPSC derived from them. We report that the cultured fibroblasts obtained from different human subjects, share comparable concentrations of proteins, RNA, DNA, and lipids in the molecular composition of nucleoli. The nucleolar molecular environment is drastically changed in the corresponding iPSC. We measured that the transition from skin fibroblasts to iPSC is accompanied by a statistically significant increase in protein concentrations ~1.3-fold, RNA concentrations ~1.3-fold, and DNA concentrations ~1.4-fold, while no statistically significant difference was found for the lipid concentrations. The analysis of molecular vibrations associated with diverse aminoacids and protein conformations indicates that nucleoli of skin fibroblasts contain similar subsets of proteins, with prevalence of tyrosine. In iPSC, we observed a higher signal from tryptophan with an increase in the random coil and α helix protein conformations, indicating changes in the subset of nucleolar proteins during cell reprogramming. At the same time, the concentrations of major types of macromolecules and protein conformations in the nucleoli of iPSC and human embryonic stem cells (hESC) were found to be similar. We discuss these results in the context of nucleolar function and conclude that the nucleolar molecular content is correlated with the cellular differentiation status. The approach described here shows the potential for spectroscopically monitoring changes in macromolecular organization of the cell at different stages of reprogramming.

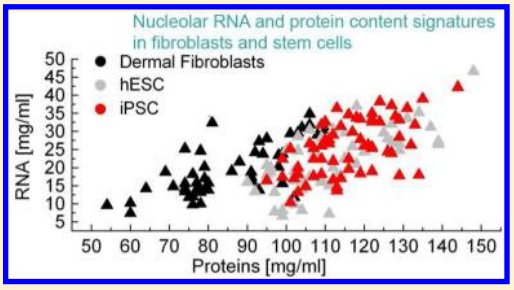

Stem cells research has been rapidly advancing since the first human embryonic stem cell (hESC) cultures were established in 1998.[1] The hESCs are pluripotent as they can differentiate into any of the more than 200 different cell types in an adult human body. The differentiation plasticity of pluripotent stem cells holds the promise for the replenishment of dead or malfunctioning cells in various tissues and organs, thus offering a new path of cure for multiple genetic and degenerative diseases. At the same time, the establishment of new hESC lines requires the destruction of human embryo, which has raised very sensitive ethical concerns and limited the development of stem cell therapies. Incomplete biocompatibility of donor stem cells with recipients' immune systems is another obstacle in hESC applications. In addition, many of the currently available hESC lines originate from unknown or insufficiently characterized sources, leading to uncertainties in selection of optimal disease- and patient-specific cells.

Recently, the concern over the human embryos, as the sole source of the human pluripotent stem cells has been overcome. The breakthrough discovery of Takahashi and Yamanaka[2,3] allowed for genetic reprogramming of adult somatic cells, such as skin fibroblasts, into hESC-alike cell lineages, namely, induced pluripotent stem cells (iPSC). It has been experimentally proven and broadly accepted that the iPSC technology generates undifferentiated cells that emulate hESC; moreover iPSC generation can be customized to obtain disease-specific and patient-specific cellular lineages.[4−6] At the same time, several problems in the iPSC induction and culturing procedures have recently become apparent. First, there is a significant variability in the dynamics of reprogramming of individual cultured cells, producing the iPSC intermediate phenotypes in cell culture.[7] Second, even in the confirmed stem cells lineages, iPSC exhibit higher heterogeneity in gene expression levels as compared to hESC, which may

Received: September 17, 2012
Accepted: March 4, 2013
Published: March 4, 2013

   dx.doi.org/10.1021/ac303806j | *Anal. Chem.* 2013, 85, 3545−3552

compromise reproducibility of prospective clinical applications.[8]

For monitoring the process of cellular reprogramming, the routine practice relies typically on the morphologic analysis of cells, which inherently is neither precise nor comprehensive. Other methods, such as fluorescence labeling of biomarkers, RT-PCR or microarray analysis can be accurate and quantitative but are by nature invasive; they disrupt the cell culture, involve cell fixation and are time-consuming, which limits their practical value. At the present time, there is a lack of quantitative technologies for noninvasive and rapid characterization, and real-time monitoring of cellular reprogramming. On the way to develop such an approach, we apply here high resolution Raman microspectrometry for identification of iPSC phenotypes.

Vibrational Raman spectroscopy utilizes inelastic light scattering on the molecular vibrations of a substance. Different molecular bonds produce their characteristic spectral lines and bands, enabling for identification of major types of biomolecules, such as proteins, RNA, DNA, and lipids in the samples. The intensity of Raman scattering response is linearly dependent on the concentration of particular molecules in the probe, which allows for quantitative measurements of molecular concentration in samples. The identification of biomolecules and their concentrations, also known as biomolecular component analysis (BCA), is based on an accurate spectral fit of a model spectrum (a linear summation of the weighted spectra of the basic components (proteins, lipids, RNA, and DNA) into a measured Raman spectrum of biological sample. The spectral weights (coefficients), which are determined during the fitting procedure, are considered as the specific contributions of the basic spectra to the resulting overall spectrum and yield directly the concentrations of basic macromolecules. Furthermore, the Raman spectra identify structural conformations of protein macromolecules.[9] Thus, BCA enables for quantitative characterization of macromolecular contents in biological samples.[10,11]

It is important to note that Raman microspectroscopy can utilize nonresonant laser sources that generate low thermal load and cause only negligible cytotoxicity, making this approach well compatible with live cell applications.[10] These advantages make Raman microspectrometry an attractive tool for monitoring cellular structural organization and biomolecular component quantification along the course of dynamic processes, such as cellular differentiation.[10,12,13]

In the stem cell field, Raman microspectrometry has been utilized in a variety of studies. These include characterization of dynamic biomolecular composition performed both in individual cells and cell colonies at different stages of differentiation,[12−18] assessment of stem cells potency,[19] identification of abnormal stem cells,[20] discrimination between hESC and their derivatives,[21,22] identification of iPSC intermediates[7] and some others (reviewed in refs 23−25). Recently, Tan et al. reported the application of Raman spectroscopy for a comparison of biomolecular organization of hESC, iPSC, and cells obtained by the non specific differentiation of hESC.[26] The probing beam was shaped to cover a relatively large area, thus averaging spectra in several cells rather than studying specificity of subcellular biomolecular composition. The authors reported an overall similarity of the hESC and iPSC Raman spectra, whereas the differentiation of hESC produced an increase in the intensity of specific lines (in the range 687−1073 cm^{-1}), which correspond to proteins, lipids, and glycogen macromolecules, thus signifying major changes of biosynthetic activities in the process of cellular differentiation.[26] However, to understand how the molecular processes in the cell are regulated, an analysis should encompass the composition of organelles that carry out specific cellular functions. In this regard, confocal Raman microspectroscopy, operating with submicrometer resolution, is capable of providing selective identification of local biochemical content in distinct subcellular regions in situ. In particular, Raman microspectroscopy identified a significant elevation of the RNA concentration in the cytoplasm of undifferentiated neural stem cells, as compared to cells of neuroglia, thus introducing a potential marker for label-free monitoring the cellular differentiation status.[13] Moreover, Raman microspectroscopy has already been validated for the analysis of even submicrometer cellular domains, such as metaphase chromosomes, including specific chromosomal bands, interbands, and telomere regions.[27,28] Confocal Raman probing of mitochondria,[29,30] lipid droplets in cytoplasm,[31] and specific structure−function compartments of the cell nucleus[10] provided unique insight into the macromolecular processes associated with these cellular domains.

In this communication, we investigated how the macromolecular composition of the nucleolus responds to cellular reprogramming to produce iPSC. Morphologically, nucleolus is the most prominent nuclear compartment; visualization of the nucleoli can be easily performed by transmission light microscopy and does not require fixation or immunolabeling procedures. The molecular content of the nucleolus is exceptionally complex and comprises genomic DNA and RNA sequences, as well as up to date known over 700 types of proteins with diverse functions. Nucleolar proteome includes proteins participating in biogenesis of ribosomes, chromatin modification factors, protein kinases and phosphatases, cell cycle regulation proteins, ubiquitin related proteins, DNA repair proteins and multiple novel, yet uncharacterized proteins.[32,33] It has also been shown that the content of nucleolar proteome is dynamic; a subset of nucleolar proteins could be transformed along with cellular regulation.[33]

Correlation of the biogenesis of ribosomes, which is a major nucleolar function with the cellular differentiation is not clear. On one hand, substantially higher levels of ribosomal genes transcription in undifferentiated and stem cells, as compared to the differentiated cells, have been shown.[34−38] On the other hand, gene array screening identified ribosomal proteins among the most stably expressed genes in the human genome in a variety of different tissues, including stem cells.[39] We believe that a spectroscopic analysis of nucleoli can contribute to understanding of correlation between content of this nuclear domain and the cellular differentiation status.

Earlier we showed the utility of Raman microspectroscopy for interrogation of molecular composition of nucleolus in situ.[10,40] In this study, we applied Raman microspectroscopy for rapid and noninvasive characterization of proteins, nucleic acids and lipids contents in the nucleoli of skin fibroblasts and stem cells. Four lines of live cultured skin fibroblasts, iPSC derived from them, and two hESC lines, were studied and compared. Our results show that the molecular composition of the nucleolar domain is dependent on the differentiation state of the cells. In all lines of cultured skin fibroblasts, the molecular compositions of the nucleoli were analogous, despite their origin from different human subjects. After these skin fibroblasts were reprogrammed to iPSC, the concentrations of

dx.doi.org/10.1021/ac303806j | Anal. Chem. 2013, 85, 3545−3552

proteins, RNA and DNA, as well as the proteins conformation patterns in nucleoli were significantly changed. We report also that the Raman signature spectra in the nucleoli of iPSC are very similar to those of hESC. We propose that the molecular content of the nucleolus provides a useful hallmark for the identification and characterization of iPSC in differentiating live cell cultures.

MATERIALS AND METHODS

Cultured Cells, Microspectroscopy. Dermal fibroblasts were obtained from skin punch biopsies from two Parkinson ' s disease patients and with parkin mutations (designated here as nP001 and nP002) and two normal subjects (designated here as nC001 and nC002). Dermal fibroblasts nP001, nP002, nC001, and nC002 were reprogrammed to iPSCs using lentiviruses expressing human Oct4, Sox2, Klf4, c-Myc, and Nanog and designated here as iP001, iP002, iC001, and iC002 respectively, see ref 41 for details. During Raman microspectrometry investigation, cells were maintained at 37 °C and 5% CO_2 in a Live-Cell incubator (Pathology Devices) mounted at the microscope stage. For spectral acquisition, nucleolar domains were located using transmission light microscopy. In control experiments, identification of the nucleoli by transmission light microscopy was validated with fluorescence imaging of nucleolar protein, nucleolin.

Raman Microspectrometry: Instrumentation, Calibration, and Data Analysis. Our custom-made confocal Raman microspectrometer is based on an inverted Nikon TE200 microscope equipped with a He−Ne (Coherent, 632.8 nm) excitation laser, fiber-input MS3501i imaging monochromator/spectrograph (Solar TII), and Hamamtsu S9974 series CCD cooled down to −60 °C.[10,40] This configuration provides the Raman spectral measurement within the spectral range of 600−3000 cm^{-1}. The spectral resolution for the fixed diffraction grating position (wavenumber interval of 1210 cm^{-1}) was ∼1.5 cm^{-1}. An excitation laser beam of ∼30 mW power is focused onto the sample in a spot of ∼0.8 μm using a 100× NA = 1.3 Nikon oil-immersion objective lens. To enable signal acquisition in a confocal mode, a 100 μm pinhole was applied. The confocal parameter was estimated to be ∼1.8 μm, as shown at the Supporting Information Figure S1.

To evaluate the experimental error in spectral intensity measurements using our setup, the Raman spectra of freshly extracted white egg were analyzed. White egg represents a highly uniform medium, composed mostly of diverse proteins and is convenient for verification of Raman spectrometer measurement accuracy in biological samples. The verification yielded an experimental error of Raman spectral intensity ∼2−5%, at the Raman shift range within 700−1700 cm^{-1} (Supporting Information Figure S2).

The integration time for Raman spectral measurements was 180 s for all experiments. Each measurement was repeated 3 times, and the signal was averaged for noise reduction. To ensure the absence of vibration, thermal drift, or other motion in our system during experiments, we visually verified the *XYZ* position of the cell before and after each measurement. Our spectroscopic studies performed in live cells did not produce any visible changes in cellular morphology[10] and showed no cytotoxicity by standard cell viability tests.

All Raman spectra were preprocessed using background subtraction, Savitzky−Golay smoothing (2nd order of polynom and 13 points of smoothing) and baseline correction.

Background elimination was performed by subtraction of the Raman spectra of incubation medium and background equalization of measured spectrum and corresponding model.[40] Examples of measured, preprocessed and analyzed Raman spectra and approaches to the background subtraction are shown in Supporting Information Figure S6−S7. Raman spectral concentration calibration was performed using bovine serum albumin, calf thymus DNA, *Saccharomyces cerevisiae* RNA and bovine heart lipids; the details are provided in our earlier study.[10] The number of measurements ranged from 11 to 37 cells for each studied cell line (Supporting Information Table S1). Measurements were averaged for each studied cell line and statistically analyzed by using a one-way ANOVA single test to find out whether two populations of the same parameter (concentration of each type of biomolecules in fibroblasts and corresponding iPSC) have the same mean value. Data of statistical analysis are presented in the Supporting Information Tables S2 and S3.

RESULTS AND DISCUSSION

Biomolecular Component Analysis of Nucleolus. Reprogramming somatic cells to iPSC triggers radical changes in cellular biosynthetic activities;[42] these changes provide potential hallmarks that could be resolved and monitored by Raman spectroscopy. Here, we investigated the impact of cellular reprogramming on the molecular content of nucleoli. Raman spectrometry analysis utilized BCA and a linear combination spectral modeling (LCSM).[10,11,43−45]

Raman spectra were acquired using confocal Raman spectroscopy setup in the central parts of nucleoli of cultured cells (see Supporting Information Figure S4) and the acquired spectra were processed as described in Materials and Methods.

The model spectrum was simulated as a best fit to the experimental spectrum through a linear combination of weighted reference spectra of the basic classes of biomolecules such as proteins, DNA, RNA and lipids.[10] A numerical value of the fractional contribution (weight) of each biomolecular component of the model Raman spectrum was assigned to the concentration of macromolecules in the nucleolus for further analysis.[10] In our modeling approach, we have used the reference spectra of cellular DNA, RNA, and lipids, the Raman spectra of calf thymus DNA, *S. cerevisiae* RNA and bovine heart lipid extract, respectively (Supporting Information Figure S3).[10] These spectra are regarded to be very close across the entire family of each type of biomolecules under diverse biological species (Supporting Information Figure S3). At the same time, the high diversity of nucleolar proteins,[33,46] with different amminoacid composition and conformations, makes the selection of a universal standard for proteins a highly problematic task. To analyze the contribution of protein constituents to the measured Raman spectra, we adopted an approach described in our earlier study.[40] Briefly, the subtraction of the linear combination of the DNA, RNA, and lipids weighted reference spectra from the acquired Raman spectrum produces a spectral profile, which represents mostly proteins and which therefore was approximated as the "nucleolar proteins" spectrum. Averaged by the number of measurements, this spectral profile may serve as an optimal model component of nucleolar proteins. Besides proteins, this spectrum includes contributions of small organic and non-organic molecules, as well as unaccounted variations of RNA, DNA, lipids spectra, that is, residual that emerges from the mismatches between measured spectrum and its model.

dx.doi.org/10.1021/ac303806j | *Anal. Chem.* 2013, 85, 3545−3552

However, considering that proteins comprise 70−80% of the dry weight of nucleoli,[47,48] we analyzed vibration frequencies of the "nucleolar proteins" spectrum correspondingly. In this analysis spectra were normalized to phenylalanine Raman peak at 1004 cm^{-1}.

It should be noted, that the contribution of saccharides (another remaining type of biomolecules) to the nucleolar Raman spectra was found to be negligible; therefore, the saccharides were not considered in our LCSM. The division of complex measured Raman spectrum into constituent spectra of major types of macromolecules is illustrated in the Figure 1.

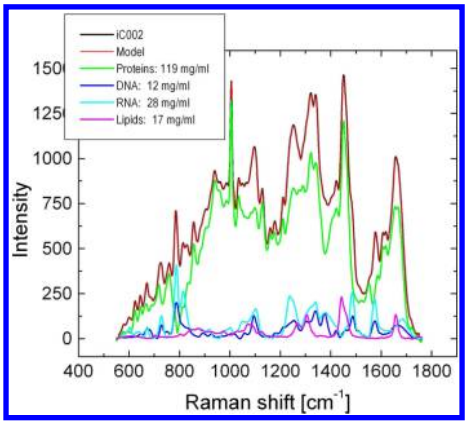

Figure 1. Application of the LCSM for BCA of nucleolus. (A) Spectrum acquired in the nucleolus of iPSC (black) laid out into component spectra of protein (green), DNA (blue), RNA (cyan), and lipid (magenta) molecular constituents. In the upper left corner are shown the concentrations of major types of biomolecules, derived from the BCA-LCSM analysis. The model spectrum is shown in red.

The black line represents the Raman spectrum measured in the central part of the nucleolus. Other spectral profiles represent the LCSM-BCA model, weighted components of the proteins, DNA, RNA, and lipids obtained by a computerized spectral LCSM procedure.

Comparative Analysis of the Nucleolar Molecular Content in Primary Fibroblasts iPSC and hESC. In our earlier study performed on HeLa cells, we demonstrated that the Raman spectra obtained from the same type of structure−function compartments of the cell nucleus (e.g., nucleolus, nuclear speckles DNA transcription sites, etc.) share overall similarity of the spectral profiles.[10] In this study, we focused on the transformations of the biomolecular content of nucleolus in the course of reprogramming of skin fibroblasts to the pluripotent state. Four earlier established dermal fibroblasts cell lines were selected for analysis.[41] Two cell lines (designated here as nC001 and nC002) were derived from normal human subjects. Another two lines (designated here as nP001 and nP002) were derived from Parkinson's disease patients with various parkin mutations. The latter two cell lines were selected because of their practical significance in studying Parkinson disease. The iPSC were generated from primary fibroblasts by using a standard protocol.[41] The iPSCs derived from the nC001, nC002, nP001, and nP002 skin fibroblasts were designated iC001, iC002, iP001, and iP002, respectively. As an internal control representing genuine stem cell phenotypes, the NIH-registered H1 and H9 hESC lines were used.

Raman microspectrometry was performed in the nucleoli, identified in live cultured cells by transmitted light microscopy (Supporting Information Figure S4).[49,50] Although the molecular structure organization of the nucleolus is complex and nonuniform,[51] we observed a substantial similarity between the Raman spectra acquired at randomly selected different sites of the same nucleolus.[40] This repeatability of the spectral measurements was apparently due to signal averaging within the detection area of the confocal volume (the size of the effective detection area is ∼0.8 × 0.8 μm in X−Y plane and confocal parameter ∼1.8 μm). Nevertheless, to enhance the consistency of measurements, the spectra were acquired in the larger nucleoli (>3 μm) and from their central parts only. In

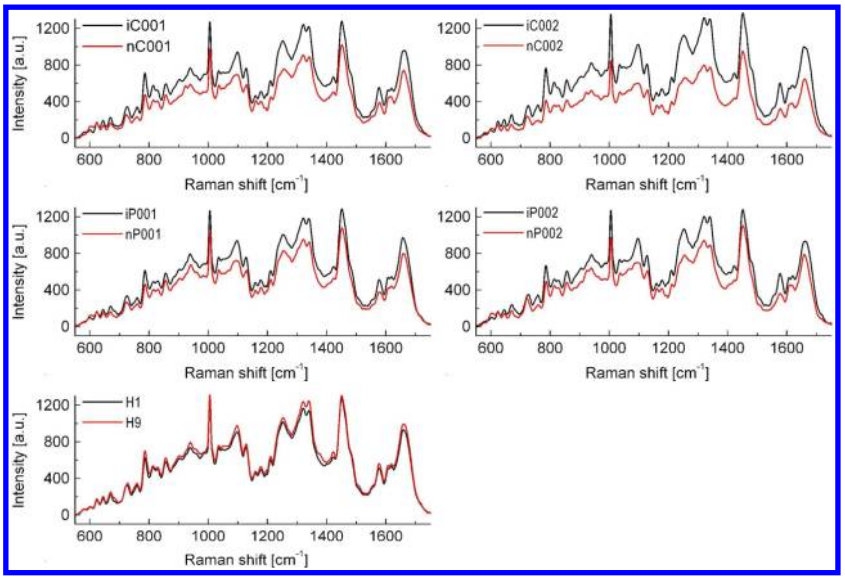

Figure 2. Overlay of Raman spectra acquired in the nucleoli of skin fibroblasts and stem cells. The figure represents the averaged nucleolar Raman spectra obtained in the skin fibroblast cell lines (nC001, nP001, nC002, and nP002) and iPSC (iC001, iP001, iC002, and iP002). The bottom left spectrum represents an overlay of averaged Raman spectra, obtained in the nucleoli of H1 and H9 hESC. The data demonstrate overall higher integral spectral intensity of the spectra acquired in the iPSC, as compared with these from the maternal skin fibroblasts cell lines. At the same time, the averaged spectra obtained for the H1 and H9 hESC were almost identical.

dx.doi.org/10.1021/ac303806j | Anal. Chem. 2013, 85, 3545−3552

each studied cell line, the Raman spectra were acquired for 11 or more cells (Supporting Information Table S1), the data were averaged and analyzed. We found that the intensities of major lines and bands of nucleolar Raman spectra could be considerably different in the skin fibroblasts, and the stem cells. Figure 2 shows the differences in the integral intensities of the spectra acquired in the nucleoli of iPSC, and their maternal dermal fibroblasts cell lines. Furthermore, the spectra acquired in the skin fibroblasts and the stem cells are clearly grouped into two segregated sets of profiles (Supporting Information Figure S5).

To interrogate these differences and to establish the contribution of proteins, DNA, RNA, and lipid groups into the spectra of dermal fibroblasts and stem cells, a BCA-LCSM approach was applied for a quantitative analysis of the nucleolar molecular composition. By matching the measured Raman spectra and the model spectra (computer generated linear combination of the concentration-calibrated reference spectra of proteins, RNA, DNA, and lipids), the concentrations of these macromolecular groups in nucleoli were determined.[10,40]

The BCA-LCSM analysis established a substantial similarity in the nucleolar macromolecular contents in all fibroblast cell lines, despite the differences in their origin. The measured concentrations of the macromolecules in the nucleoli of different cell lines are presented in Figure 3 (see also Supporting Information Figures S8 and S9 for distribution of values in individual cells). For clarity of data presentation, the concentrations of RNA, DNA, and lipids are plotted against the concentrations of proteins. Averaged concentration values and standard deviations are also presented in the Supporting Information Table S4.

The concentrations of proteins and RNA, which represent two dominant types of nucleolar macromolecules, were measured at ~90 ± 10 mg/mL and ~19 ± 7 mg/mL respectively in the cultured fibroblast cell lines. Lipids were averaged at ~16 ± 6 mg/mL. The DNA signal was highly variable averaging at 10 ± 6.0 mg/mL for different lines of noninduced fibroblasts (Figure 3 and Supporting Information Table S4).

We found that in all the tested cell lines, reprogramming of cells iPSC caused a considerable increase in proteins, DNA and RNA concentrations. The average concentration of proteins increased to ~120 ± 10 mg/mL, the concentration of RNA increased to 26 ± 8 mg/mL. The BCA analysis of individual cells also showed a linear correlation between the RNA and the protein signals in the nucleoli (see Supporting Information Figures S7 and S8). This correlation can be due to consumption of protein and RNA macromolecules for the ribosome production. At the same time, the concentration of nucleolar DNA showed an increase to 14 ± 7 mg/mL in the iPSC. Finally, the Raman signal from the lipids in the nucleoli did not significantly change upon cellular reprogramming. We report an average lipid concentration of 15 ± 4 mg/mL in iPSC (Figure 3, Supporting Information Table S4). It is worth noting that the signal from the lipids could be attributed both to macromolecules present in the nucleolar interior,[52] as well as to the nuclear envelope and its invaginations, also known as nucleoplasmic reticulum, which can spatially interact with the nucleolus.[53]

Next, we studied whether the macromolecular contents in the nucleoli of iPSC resemble the contents of hESC. In these experiments measurements were performed on the H1 and H9 hESC cell lines. We found that the contents of the

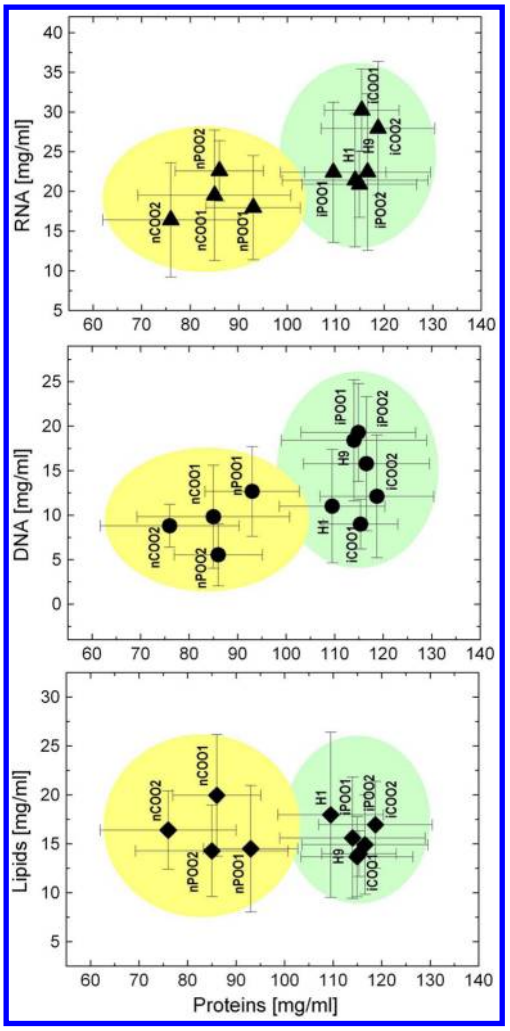

Figure 3. Concentrations of protein, RNA, DNA, and lipid macromolecules measured by BCA-LCSM in the nucleoli of fibroblasts, iPSC, and hESC. The concentrations of nucleolar proteins, DNA, RNA, and lipids were calculated in milligrams per milliliter using calibrated concentration equivalents. The data are presented as 2D plots of RNA, DNA and lipids concentrations against concentrations of proteins in each cell line. The data distribution reveals a significant difference in the nucleolar content of the two groups of cells (i.e., skin fibroblasts and stem cells including both iPSC and hESC) as indicated by the shaded areas.

macromolecules in the nucleoli of hESC and iPSC were in the same concentration ranges (Figure 3 and Supporting Information Table S4). Thus our molecular concentration mapping supports similar physiological properties of hESC and iPSC.

The averaged data for the concentrations of individual types of macromolecules in nucleoli in the groups of stem cells and skin fibroblasts are shown in the Figure 4. We found that the process of cellular reprogramming is associated with transformation of the biochemical content of nucleolus including (i) an increase in the densities of proteins and RNA by ~1.3-fold, (ii) an increase in the density of DNA by ~1.4-fold, and (iii) a slight decrease in the concentration of lipids in IPSC, although this change in lipids was not statistically significant. It could be presumed that the increase of nucleolar proteins and RNA is consistent with a substantial activation of rRNA synthesis in stem cells, reported in several studies[34−38] and thus could serve

dx.doi.org/10.1021/ac303806j | Anal. Chem. 2013, 85, 3545−3552

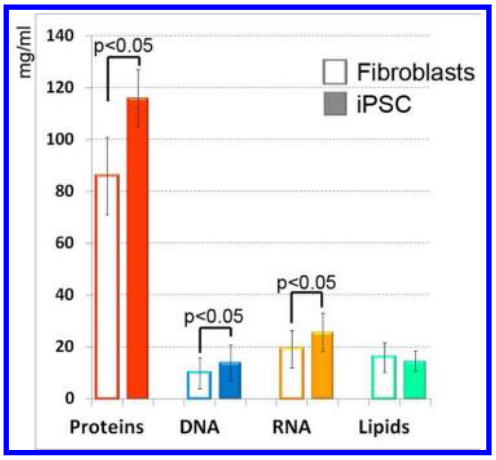

Figure 4. Averaged concentrations (in mg/mL) of proteins, RNA, DNA and lipids in the nucleoli of skin fibroblasts and stem cells. The chart represents concentration values for fibroblast in hollow collumns and values for iPSC in solid colors.St.Dev. intervals are shown. As indicated differences in the concentration of protein, DNA and RNA macromolecules were statistically significant ($p < 0.05$).

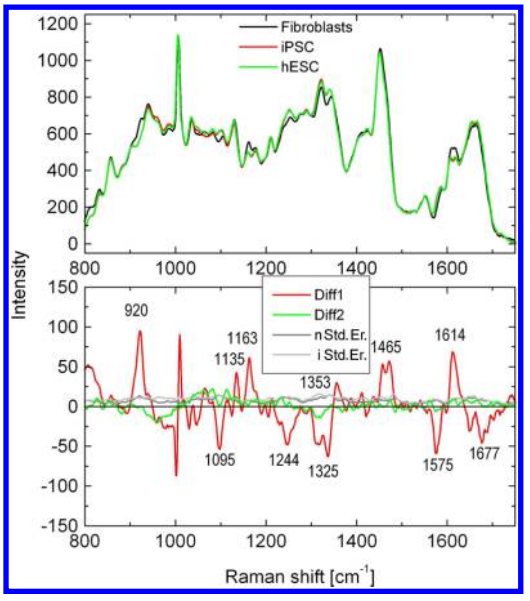

Figure 5. Analysis of proteins conformations in the nucleoli of skin fibroblasts derived from them iPSC as well as hESC cell lines. Top curves represent normalized averaged Raman spectra of nucleolar proteins components. Lower curves corresponds to (i) the profiles of spectral differences between fibroblasts and iPSC (red) and between hESC and iPSC (green) and (ii) standard error profiles (gray), calculated for each averaged curve, shown on the upper part of the graph. The difference between the upper spectral profiles was significant at the bands with the following assignments: 830 cm^{-1} and 850 cm^{-1} tyrosyl doublet due to benzene ring vibrations; 900−920 cm^{-1}, C−C stretching; 1095 cm^{-1}, alanine; 1110−1160 cm^{-1}, C−N stretching; 1163 cm^{-1}, tyrosine; 1244 cm^{-1}, amide III (random coil); 1325 cm^{-1}, CH deformations; 1465 cm^{-1}, CH_2 deformations; 1575 cm^{-1}, tryptophan ring stretch; 1614 cm^{-1}, tyrosine; 1680 cm^{-1}, amide I (random coil). See refs 56−58.

as a characteristic benchmark for stem cell phenotype. This model is also consistent with the increased size of the nucleolus, known for stem cells.[54] Notably our data on the nucleolar composition are in agreement with several studies[13,15,18,21] which reported a higher Raman intensity from nucleic acids or specifically RNA signals in the stem cells as compared to cells at various stages of differentiation. At the same time our approach yielded information on transformations in a specific nuclear compartment during the cellular reprogramming.

Besides the quantitative analysis of macromolecular concentrations, Raman microspectroscopy, together with BCA, can allow for an analysis of amino acid contents and protein conformation patterns to probe global changes in the density of constituents of nucleolar proteome. Thus spectroscopic probing of conformations of proteins present in nucleolus addresses fundamental questions: *Does the reprogramming of somatic cells to iPSC selectively change the density of specific nucleolar proteins? Do these changes in nucleolar proteome manifest themselves in specific Raman lines and bands? Finally, can specific Raman lines and bands serve as markers for identification of genuine iPSC?*

To gain insight on these questions, we performed a comparative analysis of protein constituents in different cell lines. The normalized Raman spectral profiles assigned to entire nucleolar proteome were generated, as discussed in the Biomolecular Component Analysis section. In the top part of Figure 5, colored spectral profiles for unaltered fibroblasts (black), iPSC (red) and hESC (green) cell lines are overlaid. In the bottom part of Figure 5, are shown the differences between the averaged spectra of skin fibroblasts and the iPSC (red) and between those of hESC and iPSC (green). The difference spectra on the bottom of Figure 5 were used for comparative studies of specific Raman band intensities in skin fibroblasts and stem cell lines.

The peaks at 920 and 1614 cm^{-1} are associated with the amino acid, tyrosine, and its residues in the polypeptide chains. The peaks on difference spectra, shown in the bottom of Figure 5, point to a reduced amount of this aminoacid in the nucleolar proteome of iPSC, as compared to skin fibroblast cell lines. A reduction in the tyrosine was accompanied by an increase of the tryptophan amino acid (1575 cm^{-1}) in the nucleoli of iPSC, as shown by the negative peak at the difference spectrum (Figure 5).

Next, we report a negative peak at the 1095 cm^{-1} in the difference spectrum. This band is assigned to alanine amino acid,[55] and the negative peak may signify an increase in proteins enriched with alanine in iPSC. Another possibility is that the 1095 cm^{-1} band deformation could be assigned to PO_2^- interactions of DNA molecule due to its sensitivity to the backbone geometry and to changes in the electrostatic environment of the phosphate group.[55]

Major changes at the 1440 cm^{-1} vibration band corresponding to the CH_2 side chains of proteins are also detected in iPSC. The difference spectra also indicate negative bands at 1244, 1325, and 1677 cm^{-1}. The vibrations at 1244 and 1677 cm^{-1} are associated with random coil and 1325 cm^{-1} with α-helix secondary conformations of proteins. The presence of these bands at the difference spectra points to an increase of the density of random coil and α-helix conformations in the nucleolar proteome upon reprogramming of skin fibroblasts to iPSC. Finally we documented a sharp kink at ~1004 cm^{-1}, in the difference profile between the fibroblasts and both types of stem cells -iPSC and hESC. This kink is due to a slight shift of ~1 cm^{-1} (see also an inset in Supporting Information Figure S5) of the strong and narrow protein peak, assigned to phenyl ring breathing.

At the same time, it is important to compare molecular profiles for stem cells of different origins, hESC and iPSC, to further validate iPSC applications in emerging stem cell

dx.doi.org/10.1021/ac303806j | *Anal. Chem.* 2013, 85, 3545−3552

therapies. Our study shows a close similarity between nucleolar molecular contents of hESC and iPSC types of stem cells. Mismatches between the protein spectra of hESC and iPSC were close to standard error traces (Figure 5). Thus, our comparative analysis points to a significant shift in the overall balance of nucleolar proteins during cellular reprogramming to iPSC. We found that the intensities of distinct Raman lines and bands, such as at 920 and 1614 cm^{-1} assigned to tyrosine and 1244 and 1680 cm^{-1} assigned to the random coil protein formation could be used to distinguish iPSC from skin fibroblasts. The potential significance of these lines for distinction of iPSC from iPSC intermediate phenotypes in the cell culture should be further investigated.[7] At the same time it is clear that our Raman microspectroscopy approach characterized very similar molecular environments in nucleoli of hESC and iPSC with regard to both concentration of different types of macromolecules and conformation patterns of nucleolar proteome.

CONCLUSIONS

Raman microspectrometry allows for noninvasive quantitative monitoring of the proteins, lipids, RNA and DNA concentrations in the nucleolus, as well as for probing of the nucleolar protein conformations and aminoacid variations over the course of cellular reprogramming to iPSC. Our study addresses fundamental characteristics of cellular organization and successfully complements conventional molecular biology approaches for analysis of the cellular reprogramming process. The transition from skin fibroblasts to the stem cells phenotype is accompanied by global changes in the molecular content of nucleolus, including an increase in the concentrations of proteins by ~1.3-fold, RNA by ~1.3-fold along with a DNA concentration by ~1.4-fold; on the other hand no statistically significant change in the concentrations of lipids was found. Moreover in the nucleolar proteome of iPSC we detected the decrease of tyrosine content accompanied by an increase of the tryptophan amino acid as well as increased density of random coil and α-helix conformations. We conclude that dynamics of nucleolar molecular content can serve as hallmark for the cellular differentiation status.

ASSOCIATED CONTENT

Supporting Information

Details of Raman spectra acquisition, analysis and statistical data. This material is available free of charge via the Internet at http://pubs.acs.org.

AUTHOR INFORMATION

Corresponding Author

*E-mail: pnprasad@acsu.buffalo.edu.

Author Contributions

A.P. and A.N.K. are equally contributing authors

Notes

The authors declare no competing financial interest.

ACKNOWLEDGMENTS

We thank the research subjects who participated in this study, which is approved by the Health Sciences Institutional Review Board of the State University of New York at Buffalo. The work was supported by the Air Force Office of Scientific Research, Michael J. Fox Foundation for Parkinson's Research, NYSTEM contracts C024406 and C026714, NIH grant NS061856,and SUNY REACH.

ABBREVIATIONS

iPSC	induced pluripotent stem cells
hESC	human embryonic stem cells
BCA	biomolecular component analysis
LCSM	linear combination spectral modeling

REFERENCES

(1) Thomson, J. A.; Itskovitz-Eldor, J.; Shapiro, S. S.; Waknitz, M. A.; Swiergiel, J. J.; Marshall, V. S.; Jones, J. M. *Science* **1998**, *282*, 1145−1147.

(2) Takahashi, K.; Tanabe, K.; Ohnuki, M.; Narita, M.; Ichisaka, T.; Tomoda, K.; Yamanaka, S. *Cell* **2007**, *131*, 861−872.

(3) Yu, J.; Vodyanik, M. A.; Smuga-Otto, K.; Antosiewicz-Bourget, J.; Frane, J. L.; Tian, S.; Nie, J.; Jonsdottir, G. A.; Ruotti, V.; Stewart, R.; Slukvin, I. I.; Thomson, J. A. *Science* **2007**, *318*, 1917−1920.

(4) Prasad, P. N. *Introduction to Nanomedicine and Nanobioengineering*; Wiley: Hoboken, NJ, 2012.

(5) Vogel, G. *Science* **2008**, *322*, 1766−1767.

(6) Lee, G.; Papapetrou, E. P.; Kim, H.; Chambers, S. M.; Tomishima, M. J.; Fasano, C. A.; Ganat, Y. M.; Menon, J.; Shimizu, F.; Viale, A.; Tabar, V.; Sadelain, M.; Studer, L. *Nature* **2009**, *461*, 402−U100.

(7) Chan, E. M.; Ratanasirintrawoot, S.; Park, I. H.; Manos, P. D.; Loh, Y. H.; Huo, H. G.; Miller, J. D.; Hartung, O.; Rho, J.; Ince, T. A.; Daley, G. Q.; Schlaeger, T. M. *Nat. Biotechnol.* **2009**, *27*, 1033−U1100.

(8) Narsinh, K. H.; Sun, N.; Sanchez-Freire, V.; Lee, A. S.; Almeida, P.; Hu, S. J.; Jan, T.; Wilson, K. D.; Leong, D.; Rosenberg, J.; Yao, M.; Robbins, R. C.; Wu, J. C. *J. Clin. Invest.* **2011**, *121*, 1217−1221.

(9) Chen, M. C.; Lord, R. C. *J. Am. Chem. Soc.* **1976**, *98*, 990−992.

(10) Pliss, A.; Kuzmin, A. N.; Kachynski, A. V.; Prasad, P. N. *Biophys. J.* **2010**, *99*, 3483−3491.

(11) Short, K. W.; Carpenter, S.; Freyer, J. P.; Mourant, J. R. *Biophys. J.* **2005**, *88*, 4274−4288.

(12) Konorov, S. O.; Schulze, H. G.; Atkins, C. G.; Piret, J. M.; Aparicio, S. A.; Turner, R. F. B.; Blades, M. W. *Anal. Chem.* **2011**, *83*, 6254−6258.

(13) Ghita, A.; Pascut, F. C.; Mather, M.; Sottile, V.; Notingher, I. *Anal. Chem.* **2012**, *84*, 3155−3162.

(14) Konorov, S. O.; Glover, C. H.; Piret, J. M.; Bryan, J.; Schulze, H. G.; Blades, M. W.; Turner, R. F. *Anal. Chem.* **2007**, *79*, 7221−7225.

(15) Notingher, I.; Bisson, I.; Bishop, A. E.; Randle, W. L.; Polak, J. M. P.; Hench, L. L. *Anal. Chem.* **2004**, *76*, 3185−3193.

(16) Konorov, S. O.; Schulze, H. G.; Piret, J. M.; Aparicio, S. A.; Turner, R. F.; Blades, M. W. *Appl. Spectrosc.* **2011**, *65*, 1009−1016.

(17) Zuser, E.; Chernenko, T.; Newmark, J.; Miljkovic, M.; Diem, M. *Analyst* **2010**, *135*, 3030−3033.

(18) Schulze, H. G.; Konorov, S. O.; Caron, N. J.; Piret, J. M.; Blades, M. W.; Turner, R. F. B. *Anal. Chem.* **2010**, *82*, 5020−5027.

(19) Pijanka, J. K.; Kumar, D.; Dale, T.; Yousef, I.; Parkes, G.; Untereiner, V.; Yang, Y.; Dumas, P.; Collins, D.; Manfait, M.; Sockalingum, G. D.; Forsyth, N. R.; Sule-Suso, J. *Analyst* **2010**, *135*, 3126−3132.

(20) Harkness, L.; Novikov, S. M.; Beermann, J.; Bozhevolnyi, S. I.; Kassem, M. *Stem Cells Dev.* **2012**, *21*, 2152−2159.

(21) Chan, J. W.; Lieu, D. K.; Huser, T.; Li, R. A. *Cell Res.* **2008**, *18*, S130 DOI: 10.1038/cr.2008.220.

(22) Chan, J. W.; Lieu, D. K.; Huser, T.; Li, R. A. *Anal. Chem.* **2009**, *81*, 1324−1331.

(23) Downes, A.; Mouras, R.; Elfick, A. *J. Biomed. Biotechnol.* **2010**, No. 101864, DOI: 10.1155/2010/101864.

(24) Kudelski, A. *Talanta* **2008**, *76*, 1−8.

(25) Diem, M.; Miljkovic, M.; Bird, B.; Chernenko, T.; Schubert, J.; Marcsisin, E.; Mazur, A.; Kingston, E.; Zuser, E.; Papamarkakis, K.; Laver, N. *Spectrosc. Int. J.* **2012**, *27*, 463−496.

(26) Tan, Y.; Konorov, S. O.; Schulze, H. G.; Piret, J. M.; Blades, M. W.; Turner, R. F. B. *Analyst* **2012**, *137*, 4509−4515.
(27) Demul, F. F. M.; Vanwelie, A. G. M.; Otto, C.; Mud, J.; Greve, J. *J. Raman Spectrosc.* **1984**, *15*, 268−272.
(28) Puppels, G. J.; Demul, F. F. M.; Otto, C.; Greve, J.; Robertnicoud, M.; Arndtjovin, D. J.; Jovin, T. M. *Nature* **1990**, *347*, 301−303.
(29) Matthaus, C.; Chernenko, T.; Newmark, J. A.; Warner, C. M.; Diem, M. *Biophys. J.* **2007**, *93*, 668−673.
(30) Tang, H.; Yao, H.; Wang, G.; Wang, Y.; Li, Y. Q.; Feng, M. *Opt. Express* **2007**, *15*, 12708−12716.
(31) den Hartigh, L. J.; Connolly-Rohrbach, J. E.; Fore, S.; Huser, T. R.; Rutledge, J. C. *J. Immunol.* **2010**, *184*, 3927−3936.
(32) Staub, E.; Mackowiak, S.; Vingron, M. *Genome Biol.* **2006**, *7*, No. R98, DOI: 10.1186/gb-2006-7-10-r98.
(33) Andersen, J. S.; Lam, Y. W.; Leung, A. K.; Ong, S. E.; Lyon, C. E.; Lamond, A. I.; Mann, M. *Nature* **2005**, *433*, 77−83.
(34) Thorrez, L.; Van Deun, K.; Tranchevent, L. C.; Van Lommel, L.; Engelen, K.; Marchal, K.; Moreau, Y.; Van Mechelen, I.; Schuit, F. *Plos One* **2008**, DOI: 10.1371/journal.pone.0001854.
(35) Richards, M.; Tan, S. P.; Tan, J. H.; Chan, W. K.; Bongso, A. *Stem Cells* **2003**, *22*, 51−64.
(36) Lopes, S. M. C. D. S.; Roelen, B. A. J. *Histol. Histopathol.* **2010**, *25*, 267−276.
(37) Mayer, C.; Grummt, I. *Oncogene* **2006**, *25*, 6384−6391.
(38) Bowman, L. H. *Dev. Biol.* **1987**, *119*, 152−163.
(39) de Jonge, H. J.; Fehrmann, R. S.; de Bont, E. S.; Hofstra, R. M.; Gerbens, F.; Kamps, W. A.; de Vries, E. G.; van der Zee, A. G.; te Meerman, G. J.; ter Elst, A. *PLoS One* **2007**, *2*, No. e898.
(40) Kuzmin, A. N.; Pliss, A.; Kachynski, A. V. *J. Raman Spectrosc.* **2012**, *44*, 198−204.
(41) Jiang, H.; Ren, Y.; Yuen, E. Y.; Zhong, P.; Ghaedi, M.; Hu, Z.; Azabdaftari, G.; Nakaso, K.; Yan, Z.; Feng, J. *Nat. Commun.* **2012**, *3*, 668.
(42) Takahashi, K.; Yamanaka, S. *Cell* **2006**, *126*, 663−676.
(43) Buschman, H. P.; Deinum, G.; Motz, J. T.; Fitzmaurice, M.; Kramer, J. R.; van der Laarse, A.; Bruschke, A. V.; Feld, M. S. *Cardiovasc. Pathol.* **2001**, *10*, 69−82.
(44) Shafer-Peltier, K. E.; Haka, A. S.; Fitzmaurice, M.; Crowe, J.; Myles, J.; Dasari, R. R.; Feld, M. S. *J. Raman Spectrosc.* **2002**, *33*, 552−563.
(45) Haka, A. S.; Shafer-Peltier, K. E.; Fitzmaurice, M.; Crowe, J.; Dasari, R. R.; Feld, M. S. *Proc. Natl. Acad. Sci. U.S.A.* **2005**, *102*, 12371−12376.
(46) Scherl, A.; Coute, Y.; Deon, C.; Calle, A.; Kindbeiter, K.; Sanchez, J. C.; Greco, A.; Hochstrasser, D.; Diaz, J. J. *Mol. Biol. Cell* **2002**, *13*, 4100−4109.
(47) Grogan, D. E.; Desjardi., R.; Busch, H. *Cancer Res.* **1966**, *26*, 775.
(48) Birnstiel, M. L.; Chipchase, M. I.; Flamm, W. G. *Biochim. Biophys. Acta* **1964**, *87*, 111−122.
(49) Lam, Y. W.; Trinkle-Mulcahy, L.; Lamond, A. I. *J. Cell Sci.* **2005**, *118*, 1335−1337.
(50) Busch, H.; Smetana, K. *The Nucleolus*; Academic Press: New York, 1970.
(51) Bartova, E.; Horakova, A. H.; Uhlirova, R.; Raska, I.; Galiova, G.; Orlova, D.; Kozubek, S. *J. Histochem. Cytochem.* **2010**, *58*, 391−403.
(52) Zaina, S.; Dossing, K. B.; Lindholm, M. W.; Lund, G. *Curr. Opin. Lipidol.* **2005**, *16*, 549−553.
(53) Malhas, A.; Goulbourne, C.; Vaux, D. J. *Trends Cell Biol.* **2011**, *21*, 362−373.
(54) Park, S. H.; Kook, M. C.; Kim, E. Y.; Park, S.; Lim, J. H. *Ultrastruct. Pathol.* **2004**, *28*, 229−238.
(55) Duguid, J.; Bloomfield, V. A.; Benevides, J.; Thomas, G. J. *Biophys. J.* **1993**, *65*, 1916−1928.
(56) Raso, S. W.; Clark, P. L.; Haase-Pettingell, C.; King, J.; Thomas, G. J. *J. Mol. Biol.* **2001**, *307*, 899−911.
(57) Maiti, N. C.; Apetri, M. M.; Zagorski, M. G.; Carey, P. R.; Anderson, V. E. *J. Am. Chem. Soc.* **2004**, *126*, 2399−2408.
(58) Laporte, L.; Stulz, J.; Thomas, G. J. *Biochemistry* **1997**, *36*, 8053−8059.